Shil'nikov homoclinic chaos is intimately related to type-III intermittency in isolated rabbit arteries: Role of nitric oxide

D. Parthimos, D. H. Edwards, and T. M. Griffith*
Department of Diagnostic Radiology, Wales Heart Research Institute, University of Wales College of Medicine, Heath Park, Cardiff CF14 4XN, United Kingdom
(Received 30 December 2002; published 23 May 2003)

We provide experimental evidence for the existence of Shil'nikov homoclinic chaos in the fluctuations in flow which can be observed in isolated perfused rabbit ear arteries, and establish a close association between homoclinicity and type-III Pomeau-Manneville intermittent behavior. The transition between the homoclinic scenario and type-III intermittency is clarified by a mathematical model of the arterial smooth muscle cell. Simulations of the effects of nitric oxide (NO) synthesized by the vascular endothelium on these patterns of behavior closely match experimental observations.

DOI: 10.1103/PhysRevE.67.051922 PACS number(s): 87.19.−j

The cellular mechanisms that regulate tone in the smooth muscle cells of the arterial wall are intrinsically nonlinear and generate rhythmic contractile activity (a phenomenon known as vasomotion) that can be classified as chaotic [1–3]. Indeed, previous studies have shown that a variety of established ''routes to chaos,'' including period doubling, quasiperiodicity, and Pommeau-Manneville intermittency types I and III, can be observed in the oscillatory behavior of isolated rabbit ear arteries activated by histamine [4–7]. Type-I intermittency is associated with a reverse tangent (saddle node) bifurcation in which the eigenvalues of the Floquet matrix of a fixed point pass through the unit circle, whereas type-III intermittency arises at a subcritical period-doubling bifurcation [8,9]. In both cases, the trajectories of the underlying attractor diverge from an unstable equilibrium point and are subsequently reinjected in the vicinity of the equilibrium to repeat the process. Constructions of the next-maximum return maps for the oscillations in flow that result from vasomotion have confirmed the universal features of these Pommeau-Manneville intermittency classes [6,7]. However, such an analysis reflects the local stability characteristics of the equilibrium point, rather than the nature of the reinjection regime that underpins the intermittent behavior. Here, we broaden the picture by studying the global stability properties of intermittent vasomotion in the vicinity of a homoclinic fixed point.

A homoclinic trajectory $f(x,t)$ is such that the ''inset'' to a fixed point of an attractor, x_o, is the same as the ''outset'' from the same point. It, therefore, obeys the rule that $f(x,t)\rightarrow x_o$ for $t\rightarrow\infty$, $t\rightarrow-\infty$. Homoclinic bifurcations are structurally unstable under Peixoto's theorem and are therefore destroyed by small perturbations [10]. Consequently, they are more difficult to identify than local bifurcations, since knowledge of the global properties of the phase space trajectories is required. Homoclinicity was initially studied by Rössler who identified ''spiral-'' and ''screw-'' type homoclinic scenarios [11]. Systematic characterization was, however, provided by Shil'nikov who studied homoclinicity around a saddle-focus equilibrium point [12]. In this scenario, reinjection occurs along a well-defined vector associated with a real system eigenvalue, with ejection from the vicinity of the equilibrium subsequently effected on a spiral path located on a transverse plane. A necessary condition for this mechanism is that the saddle-focus index $\delta=|\mathrm{Re}(\lambda_2)/\lambda_1|<1$, where λ_1 and λ_2 are the leading eigenvalues (λ_1 determining the rate of approaching and λ_2 determining the rate of leaving the stable point). If this Shil'nikov condition is satisfied, an infinite number of nonperiodic trajectories coexist in the vicinity of a homoclinic trajectory biasymptotic to the saddle focus. This scenario has been well documented in physicochemical systems such as the Belouzov-Zhabotinski reaction, semiconductors, lasers, and hydrodynamics [13–16], and there are limited experimental reports of such behavior in the biological context, including human brain activity and the respiratory cycle of rats [17–19].

An example of oscillations in flow induced by histamine is presented in Fig. 1(a). To establish the nature of the global dynamics of the system, the attractor underlying this time series was reconstructed by a time-delay embedding of the experimental signal, and is seen to consist of large-amplitude trajectories that are injected along a straight line into the neighborhood of a saddle equilibrium point, after which they follow an outward spiral path constrained on a plane intersecting the path of injection [Fig. 1(b)]. This scenario is in agreement with reinjection around a homoclinic point on a pleated slow manifold [Fig. 1(c)]. This mechanism is highlighted in the magnified image of the experimental signal shown in Fig. 1(a), which demonstrates that reinjection can be approximated by a convergent nonoscillatory exponential that reflects the existence of a negative real eigenvalue for the eigenvector in the reinjection direction. In contrast, the dynamics of ejection exhibits exponential oscillatory divergence associated with a pair of conjugate complex eigenvalues with positive real part such that its eigenvectors lie on the spiral plane. Estimates of these eigenvalues were obtained as $\lambda_1\sim-1.53$ and $\lambda_{2,3}\sim0.47\pm0.29i$ by exponential fitting. Importantly, the ratio $\delta=|\mathrm{Re}(\lambda_2)/\lambda_1|<1$ satisfies the condition prescribed by Shil'nikov for the existence of homoclinic chaos.

The endothelial cells that line the lumen of the arterial wall release nitric oxide (NO) which exerts an important

*Corresponding author. FAX: +44-(0)2920-744726; email address: Griffith@Cardiff.AC.UK

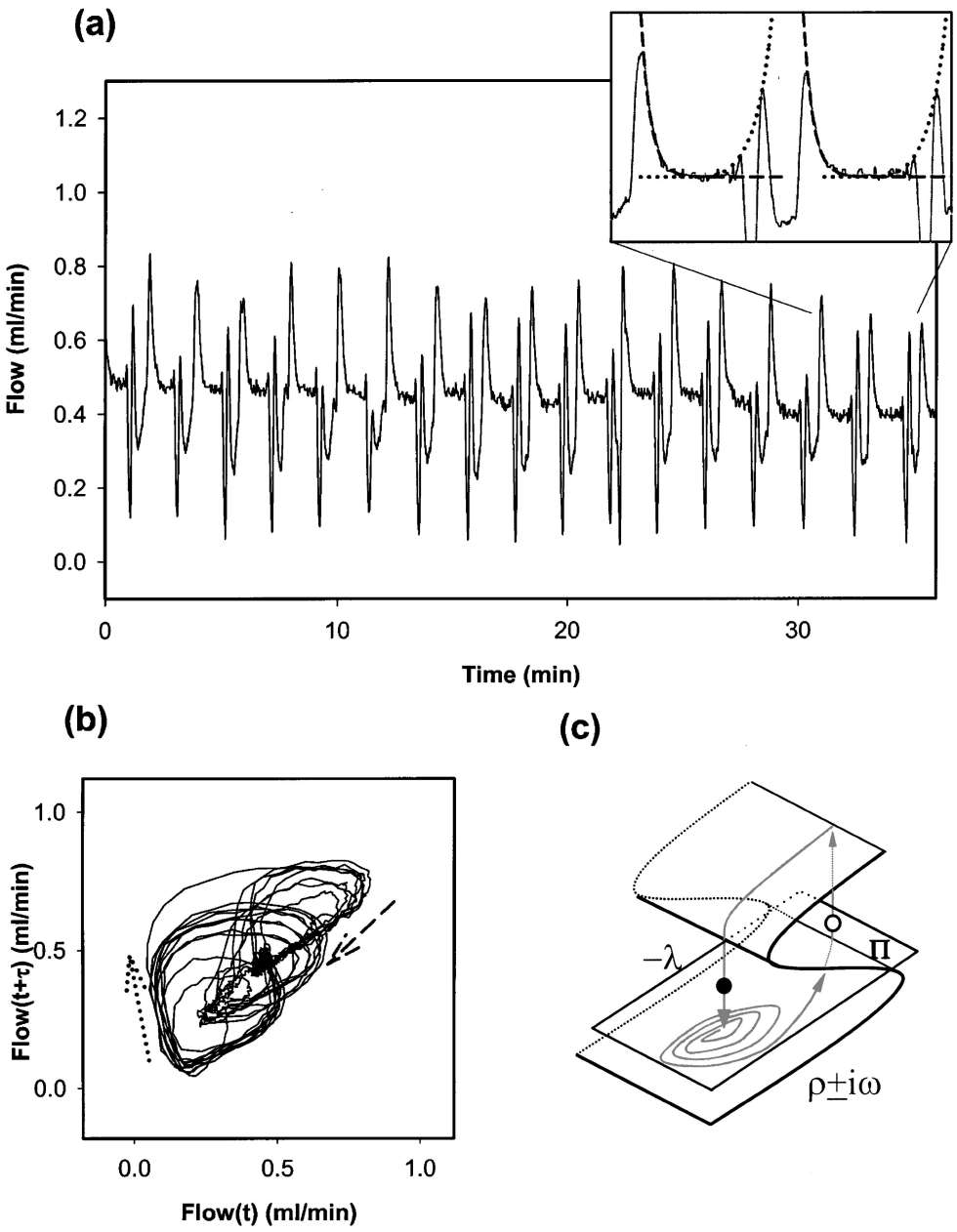

FIG. 1. (a) Oscillations in flow induced by 2.5 μM histamine in an isolated rabbit artery. A large-amplitude oscillation (dashed line) directs the time series into the vicinity of a weakly unstable locus. The time series subsequently exits this region of reduced activity via oscillations of exponentially increasing amplitude (dotted line). (b) The attractor reconstructed by time-delayed embedding of the experimental trace ($\tau=5$ sec) illustrates how trajectories are correspondingly injected into the vicinity of an equilibrium point in the direction indicated by the dashed arrow and ejected in the direction of the dotted arrow. (c) Schematic of the pleated slow manifold often associated with the reinjection mechanism of a homoclinic trajectory. The Poincaré plane Π is drawn transverse to the stable manifold (i.e., the family of the reinjection trajectories) of the attractor a short distance from a saddle focus. The points where the reinjection trajectory and the divergent oscillatory trajectory cross the Poincaré plane are indicated by closed and open circles, respectively. *Experimental methods*: Rabbit ear arteries (1–1.5 cm long, ca. 150 μm in diameter) were perfused *in situ* with oxygenated (96%O_2/5%CO_2) Holman's buffer (composition in mM: 120 NaCl, 5 KCl, 2.5 $CaCl_2$, 1.3 NaH_2PO_4, 25 $NaHCO_3$, 11 glucose, and 10 sucrose, *p*H 7.2–7.4) at 35°, as previously described [1,6,7]. An average flow was set at 0.5 ml/min, and fluctuations in flow resulting from intrinsic rhythmic vasomotor activity were monitored continuously by a Transonic systems type 2N flow probe that was included in series with the circuit immediately proximal to the artery. This probe utilizes an ultrasonic transit-time principle whereby volume flow through its sensing window is measured independent of the flow velocity profile. Superimposed variations in flow due to the perfusion pump were not evident on the experimental signals, since they were damped by an air-filled compliance chamber connected to the circuit via a sidearm proximal to the flow probe. Time series were sampled at 120 Hz. Since arterial vasomotion is characterized by oscillatory components in the range 0.001–1 Hz [1], by the Nyquist theorem this sampling rate is adequate to avoid aliasing.

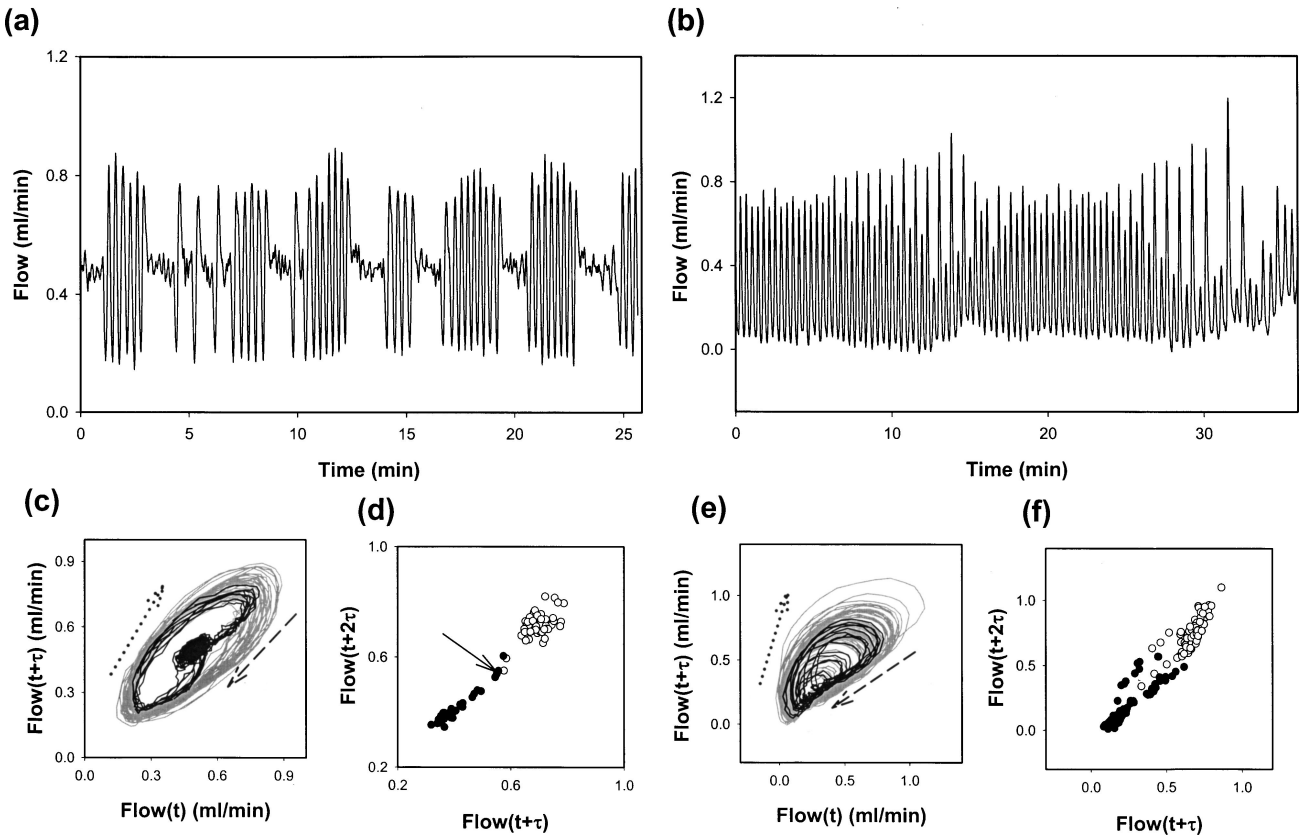

FIG. 2. Experimental vasomotion in an isolated rabbit ear artery perfused with 2.5 μM histamine (a) under control conditions and (b) in the presence of 50 μM N^G-nitro-L-arginine methyl ester (L-NAME), a compound that inhibits endothelial NO synthesis. (c) Attractor reconstructed by a time-delayed embedding of trace (a). The trajectories of the large-amplitude oscillations are shown in gray, and those of the reinjection regime in black, and follow the directions of the dotted and dashed arrows, respectively. (d) The Poincaré section through the reconstructed attractor indicating the crossings of reinjection trajectories by closed circles and crossings of trajectories leaving the plane of the unstable manifold as open circles. The arrow identifies the approximate location of the equilibrium point. (e) and (f) correspond to (c) and (d), respectively, for trace (b).

modulatory effect on the contractile behavior of vascular smooth muscle cells. However, this endogenous relaxing factor does not affect the intrinsic complexity of vasomotion as assessed by calculation of the Grassberger-Proccacia correlation dimension [1–3]. Representative examples of oscillatory activity in an isolated rabbit artery before and after suppression of NO synthesis are shown in Figs. 2(a) and 2(b), respectively. Figure 2(a) reproduces the general features of Fig. 1(a), whereas Fig. 2(b) illustrates a subharmonic bifurcation consisting of the alternating expanding and contacting modes that typify type-III Pomeau-Manneville intermittency [6,8,9]. The attractor in Fig. 2(c), reconstructed from Fig. 2(a), is dynamically equivalent to that shown in Fig. 1(b), consisting of large-amplitude trajectories injected into the neighborhood of an equilibrium point, which subsequently diverge in a spiral fashion. The attractor of vasomotion after inhibition of NO synthesis [Fig. 2(e)] is dominated by large-amplitude wandering trajectories, indicating a change in the stability characteristics of the equilibrium point around which the homoclinic point shown in Fig. 2(d) was constructed. These conclusions are supported by inspection of the Poincaré sections of the reinjection trajectories on a transverse plane lying just above the equilibrium point or its ghost [analogous to plane Π in Fig. 1(c)]. Since the reinjection trajectories follow approximately straight lines as a consequence of the Shil'nikov condition, the Poincaré section essentially mirrors the edge of the pleat manifold overlying the homoclinic reinjection focus. Thus, the homoclinic case presented in Fig. 2(d) shows an edge that reinjects trajectories always to the left of the equilibrium point (which can be identified approximately by the small-amplitude region of the corresponding time series and is indicated by an arrow). This configuration confirms homoclinicity of ''spiral type'' as characterized by Rössler [11]. Figure 2(f) shows the Poincaré section for Fig. 2(b). It is evident that reinjection now occurs along two distinct lines (sequences of closed circles), which result from an apparent bifurcation of the original simple pleat manifold. Note that localization of the equilibrium point is not possible in this case, supporting the assumption that it has become unstable in all directions and no longer maintains the Shil'nikov condition for homoclinicity.

To gain insights into the dynamical basis of the transition from homoclinicity to intermittency, associated with the suppression of NO synthesis evident in Fig. 2, simulations were performed with a previously developed mathematical model of arterial vasomotion (see the Appendix). The model generates irregular rhythmic activity through the nonlinear interaction of intracellular and membrane oscillators that govern

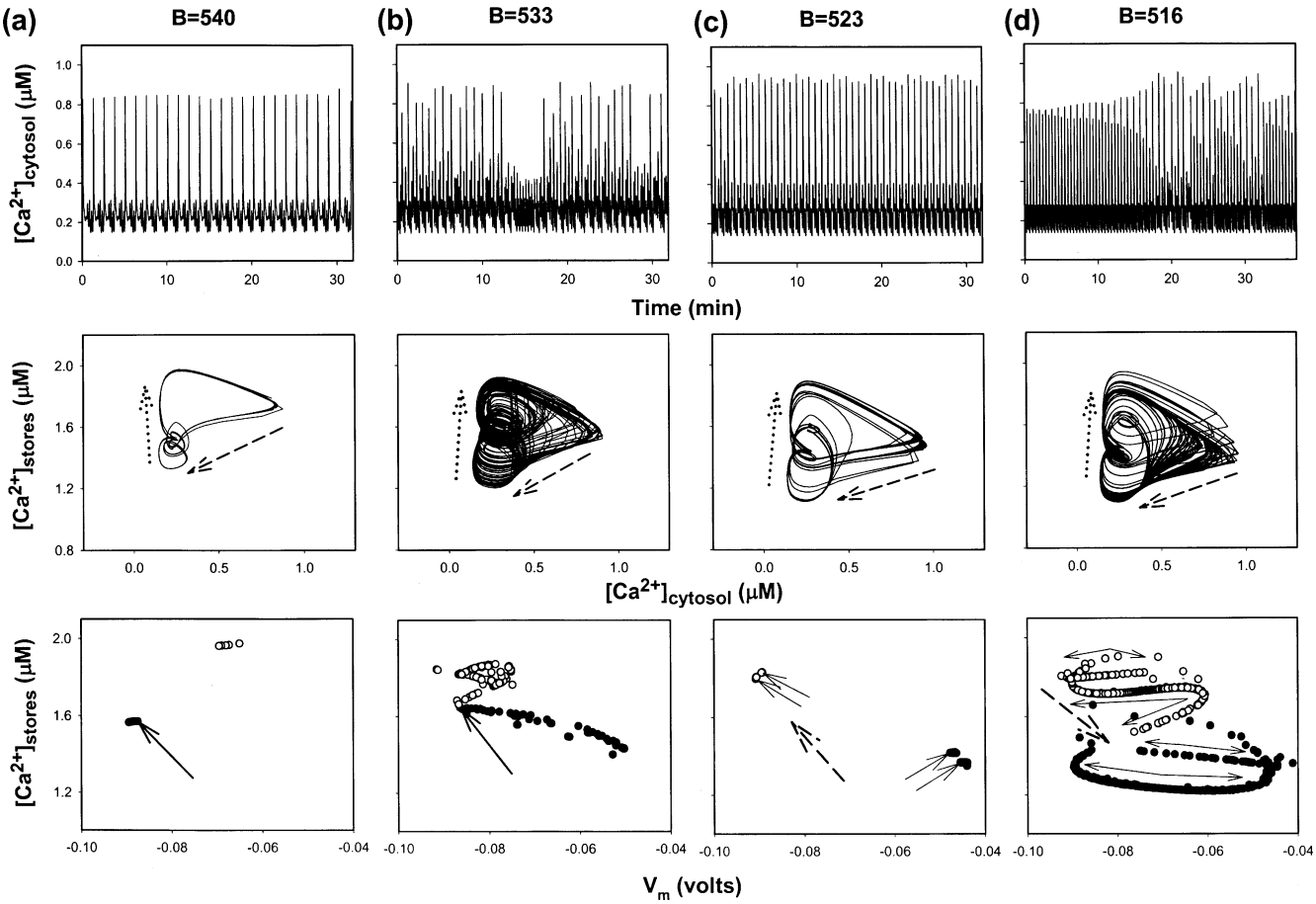

FIG. 3. Four simulations clarifying the transition from oscillatory behavior of the type illustrated in Fig. 2(a) to the type-III intermittent dynamics of Fig. 2(b) on reducing the parameter B [Eqs. (A1a) and (A1b), Appendix] from 540 to 516. This parameter governs the rate of uptake of Ca^{2+} from the cytosol into intracellular stores, which is the dominant mechanism through which NO modulates contractile activity in rabbit arteries [25]. In case (a), where the equilibrium point is strongly attractive in the direction of reinjection, the dynamics is simply a homoclinic trajectory that intersects the Poincaré section in the vicinity of the point indicated by a solid arrow. In case (b), where the dynamics is clearly chaotic, the homoclinic reinjection is extended along the edge of a pleat manifold [compare with Fig. 2(d)]. The center of the four-dimensional saddle is indicated by a solid arrow. By further reducing parameter B in case (c), the equilibrium (indicated by a dashed arrow) becomes unstable in all directions and consequently repels the trajectories that converge on a period-2 limit cycle. The points where the two folds of the new cycle intersect the Poincaré plane are indicated by closed and open circles highlighted by pairs of solid arrows. The period-2 bifurcation dynamics subsequently becomes unstable via a global bifurcation, producing divergent alternating expanding and contracting waveforms of varying duration that are characteristic of type-III intermittency (d). The stable period-2 points of the Poincaré section of case (c) are now converted into distributions of points indicated by double-edged arrows [compare with Fig. 2(f)]. The trajectories of the four-dimensional system were visualized as a projection onto the plane depicting $[Ca^{2+}]$ in the cell cytoplasm against $[Ca^{2+}]$ in intracellular stores; corresponding Poincaré sections show intersections on the plane defined by membrane potential and $[Ca^{2+}]$ in intracellular stores. Reinjection and ejection crossings of the Poincaré plane are indicated by closed and open circles, respectively.

cyclic release of Ca^{2+} from internal stores and transmembrane influx of extracellular membrane Ca^{2+} and employs four key control variables, selected on the basis of pharmacological experiments that have previously characterized histamine-induced vasomotion in rabbit ear arteries. These variables are $[Ca^{2+}]$ in the cytosol x, $[Ca^{2+}]$ in intracellular stores y, cell membrane potential z, and the open state probability of Ca^{2+}-activated K^+ channels (w), with changes in cytosolic $[Ca^{2+}]$ being equated with force development via a ''latch-bridge'' model of the contractile apparatus of smooth muscle cells [4]. Although not represented by independent dynamic variables, the model also incorporates Na^+-Ca^{2+} exchange, Ca^{2+} efflux via the membrane adenosine triphosphatase (ATP) pump and other ion transport systems. Simulations with this model reproduce a wide spectrum of experimental observations including (i) the effects of interventions that modulate the functionality of Ca^{2+} stores and membrane ion channels, (ii) paradoxes such as the unpredictable dual action of Ca^{2+} antagonists and low extracellular $[Na^+]$, which can either abolish vasomotion or promote the appearance of large-amplitude oscillations, and (iii) period-doubling, quasiperiodic, and intermittent routes to chaos [1,2,4].

In vascular smooth muscle cells, NO activity can lower cytosolic $[Ca^{2+}]$ by stimulating Ca^{2+} extrusion from the cell via the Na^+/Ca^{2+} exchanger and the membrane Ca^{2+}-ATPase pump [20–22], in addition to promoting sequestration of Ca^{2+} within intracellular stores by inhibiting

TABLE I. Eigenvalues of the equilibrium points corresponding to the simulations of Fig. 3.

	λ_1	λ_2	λ_3	λ_4
(a)	-12.5	$3.9+4.5i$	$4.1-4.7i$	2.1
(b)	-7.1	$3.3+3.4i$	$3.1-3.2i$	1.1
(c)	1.2	$3.1+3.6i$	$3.1-3.6i$	1.2
(d)	3.7	$2.4+3.5i$	$2.3-3.2i$	1.4

Ca^{2+} release from stores and enhancing store uptake of Ca^{2+} from the cytosol [23–25]. As the latter mechanism appears to dominate in rabbit arteries [25], in the present study we have modeled the effect of N^G-nitro-L-arginine methyl ester (L-NAME) by assuming that it simply reduces the term associated with store uptake, i.e., coefficient *B* in Eqs. (A1a-b), while maintaining all other coefficients in the model system constant during simulations (see the Appendix). Figure 3 illustrates four time series generated by graded changes of *B* whose attractors and associated Poincaré sections clarify the dynamic mechanisms that allow the emergence of type-III intermittency. Figure 3(a) presents a case of homoclinicity with large-amplitude oscillations being reinjected into the vicinity of a saddle-node instability. Following an initial reduction in *B*, the system contains a subset of an infinite number of chaotic trajectories regulated by a single equilibrium point located at the center of a high-dimensional saddle. This introduces an unstable limit cycle that surrounds the saddle focus and produces a mixture of large- and small-amplitude waveforms [Fig. 3(b)]. Further suppression of NO synthesis eliminates the central homoclinicity and gives prominence to an unstable large-amplitude oscillatory cycle [Fig. 3(c)], with the dynamics ultimately undergoing the subharmonic bifurcation that characterizes type-III intermittency [Fig. 3(d)].

The local stability characteristics of the model were evaluated by linearization of the system equations, with the corresponding Jacobian matrix giving the associated eigenvalues (see the Appendix and Table I). These calculations confirm that the Shil'nikov condition for homoclinicity is satisfied only for the simulations shown in Figs. 3(a) and 3(b), whereas in Figs. 3(c) and 3(d) the equilibrium point becomes unstable in all directions and no trajectories enter its vicinity. Although inhibition of NO synthesis induced a transition from homoclinicity to type-III intermittency, both experimentally and in simulations, it should be noted that it is also occasionally possible to detect type-III intermittency in the behavior of isolated arteries in the presence of basal NO activity [6]. The theoretical model would predict that in such arteries, enhancement of NO activity by additional pharmacological stimulation of the endothelium (e.g., by agents such as acetylcholine), which would be equivalent to increasing coefficient *B*, would promote the appearance of homoclinicity.

In summary, the present study has added Shil'nikov homoclinic dynamics to the patterns of vasomotion that can be observed in isolated arteries and has identified a close association with type-III intermittency. To our knowledge, homoclinicity has not previously been linked to type-III intermittency, although several studies have associated the homoclinic scenario with type-I Pomeau-Manneville intermittency or crisis-induced intermittency in physical systems such as electrical circuits [26], chemical reactions [27,28], particle physics [29,30], and flow dynamics [31]. *In vivo*, vasomotion is thought to enhance microvascular mass transport, promote lymphatic drainage, and maintain tissue perfusion when supply pressure is low, e.g., during haemorrhagic shock [32–34]. While simple sinusoidal perfusion has been shown to preserve renal function when aortic blood flow is surgically restricted [35], a specific role for more complex nonlinear patterns of response may be to allow the system to select between patterns of behavior which confer additional physiological benefit [36]. This hypothesis may be particularly relevant in the homoclinic scenario, where an infinite sequence of saddle-node and period-doubling bifurcations and their corresponding unstable trajectories coexist in the vicinity of the homoclinic singularity. It remains to be determined if the ability to select such patterns of response is impaired in disease states where NO activity may be depressed.

APPENDIX

Time gradients of the four interdependent dominant cellular parameters that regulate cytosolic Ca^{2+} in rabbit vascular smooth muscle cells are described by the following system of differential equations as presented in Ref. [4].

(*i*) *Intracellular oscillator:*

Free $[Ca^{2+}]$ in the cytosol

$$\frac{dx}{dt} = \underbrace{A_0}_{\substack{\text{Constant } Ca^{2+} \\ \text{influx through} \\ \text{receptor operated} \\ \text{channels}}} + \underbrace{A_1}_{\substack{Ca^{2+} \text{ release} \\ \text{from } InsP_3\text{-} \\ \text{sensitive stores}}} - \underbrace{G_{Ca}\,\frac{z - z_{Ca_1}}{1 + e^{-(z - z_{Ca_2})/R_{Ca}}}}_{\substack{Ca^{2+} \text{ influx} \\ \text{through voltage} \\ \text{operated channels}}} + \underbrace{G_{Na/Ca}\frac{x}{x + x_{Na/Ca}}(z - z_{Na/Ca})}_{\substack{Na^+/Ca^{2+} \\ \text{exchange}}}$$

$$\underbrace{-B\,\frac{x^n}{x^n + x_b^n}}_{\substack{\text{uptake} \\ \text{into stores}}} + \underbrace{C\,\frac{y^m}{y^m + y_c^m}\,\frac{x^p}{x^p + x_c^p}}_{\substack{Ca^{2+} \text{ induced} \\ Ca^{2+} \text{ release} \\ \text{(CICR)}}} - \underbrace{Dx^q\left(1 + \frac{z - z_d}{R_d}\right)}_{\substack{Ca^{2+} \\ \text{extrusion}}} + \underbrace{Ly}_{\substack{\text{leak} \\ \text{from} \\ \text{stores}}}. \tag{A1a}$$

$[Ca^{2+}]$ in intracellular stores

$$\frac{dy}{dt} = B\underbrace{\frac{x^n}{x^n + x_b^n}}_{\substack{\text{uptake}\\ \text{into stores}}} - C\underbrace{\frac{y^m}{y^m + y_c^m}\frac{x^p}{x^p + x_c^p}}_{\text{CICR}} - \underbrace{Ly}_{\substack{\text{leak}\\ \text{from}\\ \text{stores}}}. \tag{A1b}$$

(ii) Membrane oscillator:

Relationship between ion fluxes and membrane potential

$$\frac{dz}{dt} = \gamma\left[-2G_{Ca}\underbrace{\frac{z - z_{Ca_1}}{1 + e^{-(z - z_{Ca_2})/R_{Ca}}}}_{\substack{Ca^{2+}\ \text{influx}\\ \text{through VOCC}}} - G_{Na/Ca}\underbrace{\frac{x}{x + x_{Na/Ca}}}_{\substack{Na^+/Ca^{2+}\\ \text{exchange}}}(z - z_{Na/Ca}) - \underbrace{G_k w(z - z_K)}_{K^+\ \text{efflux}}\right]. \tag{A1c}$$

Open state probability of K_{Ca} channels

$$\frac{dw}{dt} = \lambda\left(\underbrace{S\frac{(x + x_w)^2}{(x + x_w)^2 + \beta e^{-(z - z_{Ca_3})/R_K}}}_{\substack{Ca^{2+}\ \text{and voltage}\\ \text{activation}}} - \underbrace{w}_{\text{decay}} \right). \tag{A1d}$$

Parametric values for Eqs. (A1) maintained constant throughout the simulations were

$A_0 + A_1$:	0.475 μM/sec	G_{Ca}:	16.425 μM/V sec
$G_{Na/Ca}$:	43.8 μM/V sec	x_b:	4.47 μM
C:	6250 μM sec^{-1}	y_c:	8.9 μM
q:	2	D:	6.2 μM^{1-q}/sec
L:	0.025 sec^{-1}	γ:	0.34 V/μM
G_K:	73 μM/V sec	λ:	15
S:	1	x_w:	0.5 μM
β:	0.7 μM^2		

Variables x and y are in μM, and z in volts. The value of coefficient B (in μM sec^{-1}) was varied in simulations and is therefore given at the relevant location in the text. Reversal potentials and Hill coefficients of individual ion channels and transport mechanisms are given in Ref. [4]. Note that the complexity of the model was slightly reduced in the present study compared to its original formulation by omitting the contributions of the Na^+/K^+-ATPase and chloride channels to membrane potential.

The equilibrium points (x^*, y^*, z^*, w^*) of the system satisfy the equations

$$\left.\frac{dx}{dt}\right|_{(x^*,y^*,z^*,w^*)} = \left.\frac{dy}{dt}\right|_{(x^*,y^*,z^*,w^*)} = \left.\frac{dz}{dt}\right|_{(x^*,y^*,z^*,w^*)} = \left.\frac{dw}{dt}\right|_{(x^*,y^*,z^*,w^*)} = 0. \tag{A2}$$

Linearization of Eq. (A1a): $dx/dt = f_x(x,y,z,w)$ around the equilibrium (x^*, y^*, z^*, w^*) gives

$$\frac{d\overline{x}}{dt} = \frac{\partial f_x(\cdots)}{\partial x}\overline{x} + \frac{\partial f_x(\cdots)}{\partial y}\overline{y} + \frac{\partial f_x(\cdots)}{\partial z}\overline{z} + \frac{\partial f_x(\cdots)}{\partial w}\overline{w}, \tag{A3}$$

where $\overline{x} = x - x^*$, $\overline{y} = y - y^*$, $\overline{z} = z - z^*$, $\overline{w} = w - w^*$. A similar procedure for the other variables provides the eigenvalues specifying the stability characteristics of the system around the equilibrium point (x^*, y^*, z^*, w^*) via the Jacobian:

$$J = \left[\begin{array}{cccc} \dfrac{\partial f_x(\cdots)}{\partial x} & \dfrac{\partial f_x(\cdots)}{\partial y} & \cdots & \cdots \\ \dfrac{\partial f_y(\cdots)}{\partial x} & \dfrac{\partial f_y(\cdots)}{\partial y} & \cdots & \cdots \\ \cdots & \cdots & \cdots & \cdots \\ \cdots & \cdots & \cdots & \cdots \end{array}\right]_{(x^*,y^*,z^*,w^*)}. \tag{A4}$$

[1] T. M. Griffith and D. H. Edwards, Am. J. Physiol. **266**, H1786 (1994).

[2] T. M. Griffith and D. H. Edwards, Am. J. Physiol. **266**, H1801 (1994).

[3] T. M. Griffith and D. H. Edwards, Am. J. Physiol. **269**, H656 (1995).

[4] D. Parthimos, D. H. Edwards, and T. M. Griffith, Am. J. Physiol. **277**, H1119 (1999).

[5] S. De Brouwer, D. H. Edwards, and T. M. Griffith, Am. J. Physiol. **274**, H1315 (1998).

[6] T. M. Griffith, D. Parthimos, J. Crombie, and D. H. Edwards, Phys. Rev. E **56**, R6287 (1997).

[7] D. Parthimos, D. H. Edwards, and T. M. Griffith, Phys. Rev. E **64**, 061906 (2001).

[8] P. Manneville and Y. Pomeau, Physica D **1**, 219 (1980).
[9] Y. Pomeau and P. Manneville, Commun. Math. Phys. **74**, 189 (1980).
[10] S. K. Scott, *Chemical Chaos* (Clarendon Press, Oxford, 1991).
[11] O. E. Rössler, Bull. Math. Biol. **39**, 275 (1977).
[12] L. P. Shil'nikov, Soc. Math. Dokl. **6**, 163 (1965).
[13] F. Argoul, A. Arneodo, and P. Richetti, J. Chim. Phys. Phys.-Chim. Biol. **84**, 1367 (1987).
[14] T. W. Carr, L. Billings, I. B. Schwartz, and I. Triandaf, Physica D **147**, 59 (2000).
[15] R. Herrero, R. Pons, J. Ferjas, F. Pi, and G. Orriols, Phys. Rev. E **53**, 5627 (1996).
[16] M. J. Ablowitz, J. Hammack, D. Henderson, and C. M. Schober, Phys. Rev. Lett. **84**, 887 (2000).
[17] G. V. Wallenstein, J. A. S. Kelso, and S. L. Bressler, Physica D **84**, 626 (1995).
[18] J. A. S. Kelso and A. Fuchs, Chaos **5**, 64 (1995).
[19] M. Sammon, J. R. Romaniuk, and E. N. Bruce, J. Appl. Physiol. **75**, 912 (1993).
[20] K. Furukawa, Y. Tawada, and M. Shigekawa, J. Biol. Chem. **263**, 8058 (1988).
[21] K. Furukawa, N. Ohshima, Y. Tawada-Iwata, and M. Shigekawa, J. Biol. Chem. **266**, 12 337 (1991).
[22] L. M. Popescu, C. Panoiu, M. Hinescu, and O. Nutu, Eur. J. Pharmacol. **107**, 393 (1985).
[23] M. Hirata, K. P. Kohse, C. H. Chang, T. Ikebe, and F. Murad, J. Biol. Chem. **25**, 1268 (1990).
[24] J. Z. Yu, D. X. Zhang, A. P. Zou, W. B. Campbell, and P. L. Li, Am. J. Physiol. **279**, H873 (2000).
[25] R. A. Cohen, R. M. Weisbrod, M. Gericke, M. Yaghoubi, C. Bierl, and V. M. Bolotina, Circ. Res. **84**, 210 (1999).
[26] M. S. Baptista and I. L. Caldas, Physica D **132**, 325 (1999).
[27] P. Richetti, F. Argoul, and A. Arneodo, Phys. Rev. A **34**, 726 (1986).
[28] H. Herzel, P. Plath, and P. Svensson, Physica D **48**, 340 (1991).
[29] S. V. Prants, Phys. Rev. E **61**, 1386 (2000).
[30] C. L. Pando, G. Perez, and H. A. Cerdeira, Phys. Rev. E **48**, 196 (1993).
[31] A. E. Abasaeed and S. S. E. H. Elnashaie, Chaos, Solitons Fractals **9**, 455 (1998).
[32] J. A. Schmidt, M. Intaglietta and P. J. Borgström, J. Appl. Physiol. **73**, 1077 (1992).
[33] T. W. Secomb, M. Intaglietta, and J. F. Gross, Prog. Appl. Microcirc. **15**, 49 (1989).
[34] T. C. Skalak, G. W. Schmid-Schönbein, and B. W. Zweifach, Microvasc. Res. **28**, 95 (1984).
[35] B. Nafz, J. Stegemann, M. H. Bestle, N. Richter, E. Seeliger, I. Schimke, H. W. Reinhardt, and P. B. Persson, Circulation **101**, 553 (2000).
[36] D. Parthimos, D. H. Edwards, and T. M. Griffith, Cardiovasc. Res. **31**, 388 (1996).